[Frontiers in Bioscience 7, f1-7, January 1, 2002]

NEAR REAL-TIME *IN VIVO* CONFOCAL IMAGING OF MOUSE MAMMARY TUMORS

Alicia A. Lacy [1], Tom Collier [1], Janet E. Price [2], Su Dharmawardhane [3], and Rebecca Richards-Kortum [1]

[1] Biomedical Engineering Program, The University of Texas at Austin, Austin Texas 78712, [2] The University of Texas MD Anderson Cancer Center, Houston Texas 77030, [3] Molecular Cell and Developmental Biology, The University of Texas at Austin, Austin Texas 78712

TABLE OF CONTENTS

1. ABSTRACT

The goal of this study was to evaluate the ability of near real-time reflectance confocal microscopy to image tumor metastasis *in vivo* in an animal model. We used an epi-illumination confocal microscope to capture images of mouse mammary tumors in nude immunodeficient and Balb/C immunocompetent mice. *In vivo* confocal images and videos of normal and neoplastic areas were obtained before and after the application of a 6% acetic acid solution, with a lateral resolution of 0.8 microns and an axial resolution of 2-3 microns. Average imaging depths ranged from 150 microns to greater than 300 microns. We were able to differentiate between normal and abnormal tissue areas within the mammary gland, including areas of adipose tissue, fibroblasts and connective tissue, neoplastic tissue, and blood flow within blood vessels. Intravital imaging with reflectance confocal microscopy appears to be a useful tool to study tumor metastasis *in vivo*.

2. INTRODUCTION

Breast cancer is the second most commonly diagnosed cancer in women, after skin cancer, and the second leading cause of cancer death (1). However, it is the tumor metastases, rather than the primary breast tumor, that are responsible for most of these cancer deaths. Cancer metastasis is a complex multi-step process by which malignant cancer cells separate from a primary tumor, migrate through the extracellular matrix, and travel through the circulatory or lymphatic systems to establish secondary tumors at distant sites (2-6).

Until recently, a thorough analysis of the mechanisms involved in early metastatic invasion and secondary colonization has been limited by the inability to investigate cellular behavior *in vivo* in real time. Traditional studies of metastases have been based on "end point" assays, where cancer cells are injected either intravenously or subcutaneously into an appropriate host animal. The number of cells and type of cells injected (the start point) is known, and the number and sizes of metastases produced in various organ sites at specified time intervals (the end point) are assessed (3, 7). A major limitation to this method is that no knowledge is gained about the events which occur between the start and the end points. Therefore, a more informative approach is required for complete *in vivo* analysis of the complex metastatic process.

Recent advances in digital imaging and microscopy have provided means of high-resolution intravital imaging. Intravital imaging is a technique that permits direct optical examination of individual living cells and tissues *in vivo*. This technique has been used to study the events of the metastatic process that were previously inaccessible by traditional *in vivo* and *in vitro* assays. Using an inverted epi-fluorescence microscope with transillumination provided by a fiber optic light source, Ann Chambers' laboratory has investigated the entry and arrest, movement and deformation, and survival of cancer cells through the various stages of intra- and extravasation in the liver and muscle of mice (3, 7-10) and the

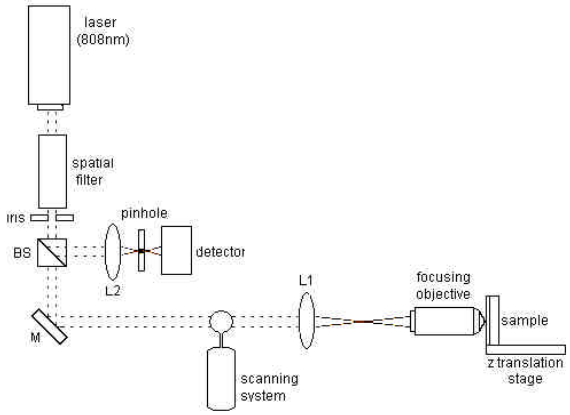

Figure 1. Setup of epi-illumination confocal microscope.

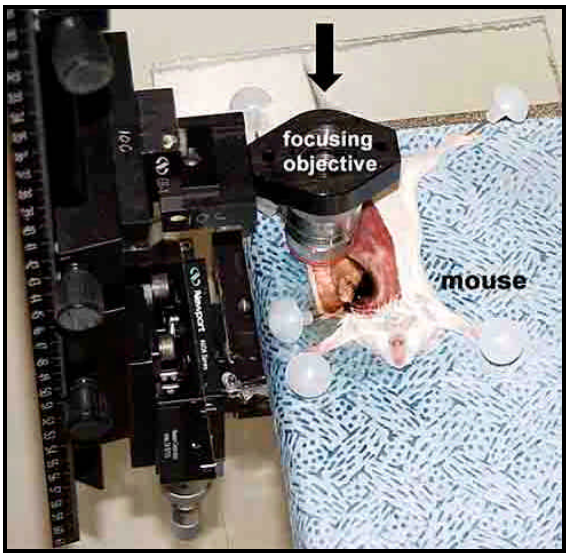

Figure 2. Picture of Balb/C mouse during imaging. The arrow indicates the direction of illumination light.

chorioallantoic microcirculation of chick embryos (3, 11). They have mixed fluorescent microspheres with untagged cells of the same diameter as a method of tracking and counting tumor cells as they lodge in the circulatory system of mice and chick embryos (3, 11). They have also used fluorescently labeled nanospheres, taken up by the cells via endocytosis (3,7), as well as green fluorescent protein (GFP)-expressing cells (9-11) to study these events. Condeelis and his colleagues have used a slit-scanning confocal microscope, with an 8 mm slit, to visualize the early motile events of metastasis at the cellular level using GFP-expressing tumor cells in rat models (4, 6, 12, 13). They were able to obtain single sections at two-minute intervals. Similar techniques have been used to obtain insight into angiogenesis and blood flow, cell adhesion, and interstitial diffusion by Jain et al. (14).

Rather than using fluorescence microcopy, we explore the use of reflectance microscopy in this study. The goal of this study was to evaluate the ability of near real-time reflectance confocal microscopy to image tumor metastasis *in vivo* in an intact tumor. Reflectance microscopy allows visualization of tumor cells in their natural state without altering their genetic make-up. With more sensitive detectors, higher speeds of image acquisition, and a confocal pinhole, we were able to significantly increase the spatial and temporal resolution of live cell imaging in intact tissue. Advances in this technique have the potential to allow in-depth study of breast cancer cells and host cells to gain a more complete understanding of cancer metastasis in the future.

3. EXPERIMENTAL METHODS

3.1. Confocal System

An epi-illumination reflectance-based confocal microscope, constructed in our lab, was used for this study (figure 1). This microscope is equipped with an 810 nm 115 mW diode light source (L2 810S-115, Microlaser) that is directed to an x-y scanning system. The scanning mirrors are driven by a pair of galvanometers to produce a frame rate of 7.5 Hz (4 kHz Video Scan Head, General Scanning). The scanning system creates a focused excitation field by raster scanning across the back aperture of a 25x 0.8NA water-immersion objective (plan-Neofluor multi-immersion, Zeiss). The objective focuses 14-30 mW of power to a spot with a 1-micron diameter onto the sample. Light reflected from the sample is descanned and recollimated by the scanning system, then focused into a pinhole aperture with a 10-micron diameter. Light passing through the pinhole is collected by an avalanche photodiode detector (APD C5460, Hamamatsu). The system has zoom capabilities, allowing a field of view ranging from 48 microns to 1 mm, and has measured lateral and axial resolutions of 0.8 microns and 2-3 microns, respectively (15).

3.2 Animals and Tumors

66.3 mouse mammary cancer cells (16) were implanted into the mammary fat pads of four female NCr-nu athymic nude (immunodeficient) mice and one female Balb/C (immunocompetent) mouse. The cells were allowed to form primary tumors, approximately 5-10 mm in diameter. The primary tumor was produced according to the method of Lachman et al. (17). Before imaging, the mice were anesthetized with 50 mg/kg Nembutol in 0.1 ml PBS, injected intraperitoneally. The tumors were surgically exposed by creating a skin flap that allowed direct viewing of the tumor while maintaining an intact blood supply to the tumor and surrounding tissues. The tumors were contained within the skin flap that was cut back; therefore the tumors were imaged from their most posterior surface (figure 2). The Institutional Animal Care and Use Committee (IACUC) at The University of Texas MD Anderson Cancer Center approved the use of the mice. After imaging, the mice were euthanized and tumor tissue was removed for subsequent histological analysis using hemotoxylin and eosin (H&E) staining.

3.3. Imaging

Pixel-based images, displayed at approximately eight frames per second on a computer monitor attached to the microscope, were saved as individual bitmaps (static

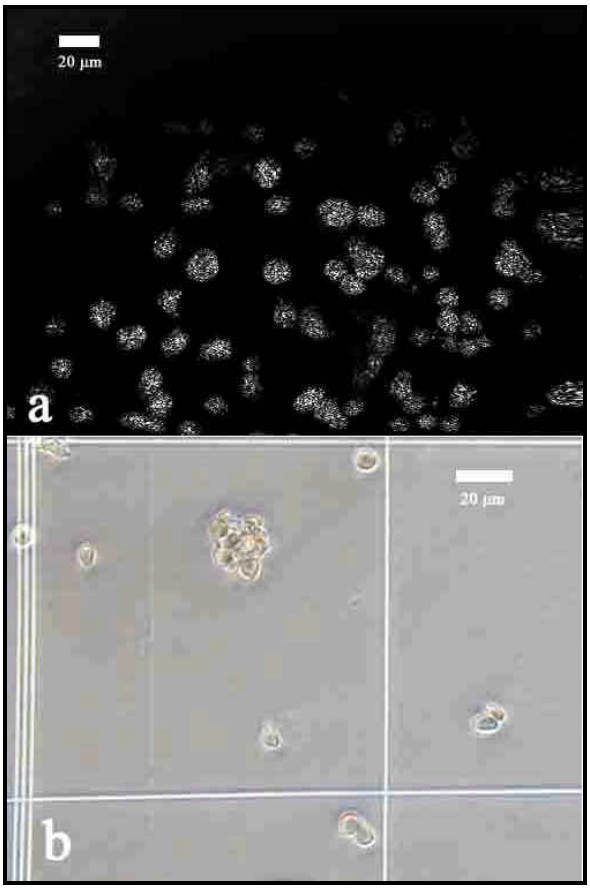

Figure 3. Type 66.3 mouse mammary cancer cells. (a) Confocal image of cells suspended on Knox Gelatin® after the application of acetic acid. (b) Phase contrast image of cells in a hemocytometer chamber.

images) and AVI video files (dynamic images). All samples were imaged before and after the topical application of a 6% acetic acid solution, a clinical contrast agent (15). We first observed the mammary cancer cells suspended on Knox Gelatin®. Then, *in vivo* confocal images and videos of both normal and neoplastic areas within the mice were acquired. Video was acquired as the microscope focus was moved from the posterior surface of the tissue flap through a z-series until no image features could be observed (greater than 300 microns in some cases).

3.4. Image Processing

The images (static and dynamic) were resampled and processed to enhance the brightness and contrast levels. The brightness and contrast were enhanced by either adding, if positive (+), or subtracting, if negative (-), the noted percentage of full gray scale to each pixel, and expanding the remaining midrange gray levels. Resampling was performed to remove distortions due to the nonlinearity of the resonant galvanometer in the scanning system. Linear interpolation was used to estimate pixel size. The videos, available for viewing at www.ece.utexas.edu/speclab/publications/publications.htm, were compressed using Cinepak Codec by Radius for Microsoft AVI and Cinepak Compression for QuickTime (Adobe Premiere 5.1).

3.5. Histology

The tumors were excised, fixed in 10% buffered formalin, embedded in paraffin, and cut into four-micron thick sections. They were then stained with hemotoxylin and eosin, for histological analysis. Each histology image shown was taken with a 10x eyepiece and either a 10x or 40x microscope objective. Thus, if the magnification noted is 100x, the 10x objective was used. If the noted magnification is 400x, the 40x objective was used.

4. RESULTS

66.3 mouse mammary cancer cells suspended on Knox Gelatin® were visualized first. Figure 3(a) shows a confocal image of the cells after the application of acetic acid. Acetic acid was used as a contrast agent to increase cell detection. In reflectance confocal images, it has been shown to cause a brightening of cell nuclei, or in some cases the entire cell, such that the nuclei cannot be distinguished from surrounding cytoplasm (15). In this case, the entire cell brightened with the addition of acetic acid. The cells appear to be 14 microns in diameter, which correlates well with the phase contrast image shown in figure 3(b). The phase contrast image was taken with a 10x objective, such that the prominent square of the hemocytometer is 0.25 mm across.

The mouse tumors were then imaged. Mouse tumors often become encapsulated by fibrous capsules, consisting of fibroblasts and extracellular matrix of the host tissue [2, 18, 19]. Figure 4(a) shows an image of the surface of a fibrous capsule in a nude mouse after the application of acetic acid. The white spots in the image are fibroblast nuclei. The blurred areas are extracellular matrix components that can be seen with more detail in figure 5. The components identified in the confocal image, the fibroblasts and matrix fibers, are also seen in the histology sections, figures (b) and (c). In the confocal image, neither the brightness nor contrast have been adjusted. Figure 5 consists of a series of static images of a typical fibrous capsule covering a tumor in a nude mouse, after the application of acetic acid. The brightness has been increased by 66% and the contrast increased by 38% in each of the 442 x 327 micron images. The white spots seen are fibroblast nuclei and the string-like structures are collagen and elastin fibers. Due to the backscattering of the light by the collagen and elastin fibers and fibroblasts, the incident signal was lost before the neoplastic cells of the tumor were imaged. This occurred in a number of the tumors we imaged. A video of a typical z-series through 135 microns of a fibrous capsule is available at www.ece.utexas.edu/speclab/publications/publications.htm. The images in figure 6 demonstrate a z-series through a normal area of tissue in a nude mouse after a 6% acetic acid solution has been applied. The plane of focus of the microscope objective was moved from the posterior surface of the normal skin tissue towards the anterior surface, to a depth of 165 microns. The field of view of each image is 442 x 327 microns. The brightness and contrast of each

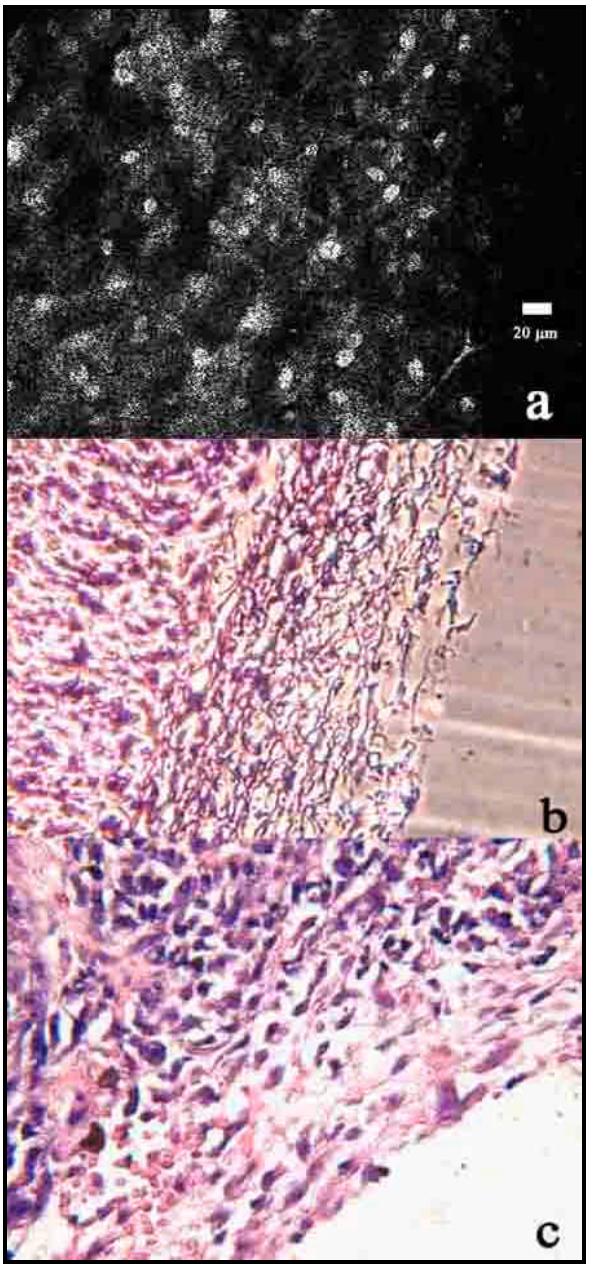

Figure 4. (a) Confocal image of fibroblasts and collagen and elastin fibers of fibrous capsule covering tumor in a nude mouse, after application of acetic acid. The field of view is 397 x 293 microns. (b and c) Histology of the fibrous capsule in the nude mouse, at 400x. The field of view is 225 x 176 microns.

image has been altered by +50% and +30%, respectively. Figures 6(a) and (b) are images of fibroblasts; (c) is a transition zone between fibroblast layers and layers of adipocytes. Large adipocytes are pictured in figures (d), (e), and (f). The corresponding video can be viewed from www.ece.utexas.edu/speclab/publications/publications.htm. Figures 7(a) and (b) show images of adipose tissue 100 microns below the imaging surface, at different magnifications after applying acetic acid. Figure (a) has a field of view of 676 x 502 microns, and the brightness and contrast have been adjusted by 0% and +50%, respectively. Adipocytes can be seen, as large open spaces, next to neighboring fibroblasts. At higher magnification, with a field of view of 380 x 262 microns and no adjustment to the brightness or contrast, the lipid droplets of the cells can be seen in figure (b). These cells are approximately 45 microns in diameter, which is similar to the histology sections shown in figures (c) and (d). In the histology sections, figures (c) and (d), the lipid droplets are seen as large, unstained spaces within each cell. This is an artifact of the fixation process, which extracts the lipid droplet causing some shrinkage of the adipocyte. Figure 8(a) shows an area of neoplastic tissue 75 microns below the imaging surface, after applying acetic acid. The sizes of the tumor cells are larger than cells of surrounding normal tissue, pictured previously in figure 6. The cells average 17 microns in diameter. This is similar to the diameter of the cells shown in matching histology (figure 8(b)) as well as the tumor cells measured previously in suspension. The brightness of image (a) has been increased by 6% and the contrast increased by 65%. The field of view is 605 x 449 microns. Figure 9 represents a z-series through 213 microns of neoplastic tissue, also after the application of acetic acid. Figures (a), (b), (c), and (d) consist mainly of the fibrous capsule surrounding the tumor. The bright spots are fibroblast nuclei and the fibers are collagen and elastin fibers. The larger bright spots in figures (f) and (g) are neoplastic cells. A video of this z-series can be viewed at www.ece.utexas.edu/speclab/publications/publications.htm. At the end of this video, necrotic tissue can be seen at the center of the field of view. Each image in figure 9 is 442 x 327 microns, and the brightness and contrast have been adjusted by +62% and +19%, respectively.

The average depth at which we were able to image differed greatly between tumors in different mice. For normal tissue with acetic acid applied, the imaging depth ranged from 155 microns to greater than 300 microns. For neoplastic tissue, the average depth of penetration was 190 microns without acetic acid and 185 microns with acetic acid. The imaging depth of the neoplastic areas depended greatly on the size of the tumor and the thickness of the fibrous capsule surrounding the tumor.

Finally, in addition to the adipose tissue of the mammary fat pad, the fibroblasts and collagen and elastin fibers of the normal tissue and fibrous capsule, and the neoplastic cells, we were also able to view other structures. Figure 10(a) shows an area of striated muscle found within the tumor, with corresponding histology pictured in figure 10(b). The brightness and contrast levels have not been adjusted. A video of blood flowing through a blood vessel near the surface of a tumor was recorded and can be viewed from www.ece.utexas.edu/speclab/publications/publications.htm.

5. DISCUSSION AND CONCLUSIONS

As can be seen in the static images presented and the dynamic videos made available on our website, with the

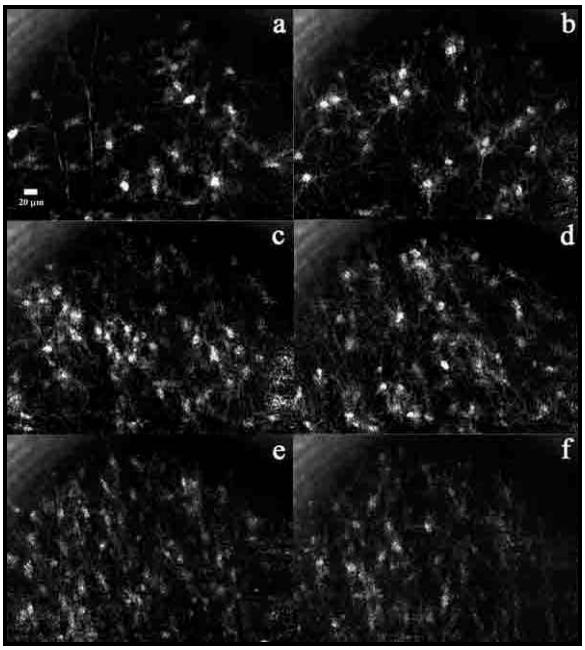

Figure 5. Images of a typical fibrous capsule covering a tumor in a nude mouse, after the application of acetic acid. The brightness has been increased by 66% and the contrast increased by 38%. The field of view is 442 x 327 microns. Image (a) is 20 microns, (b) 40 microns, (c) 60 microns, (d) 80 microns, (e) 100 microns, and (f) 120 microns beneath the tumor surface. The scale bar in figure (a) applies for all images.

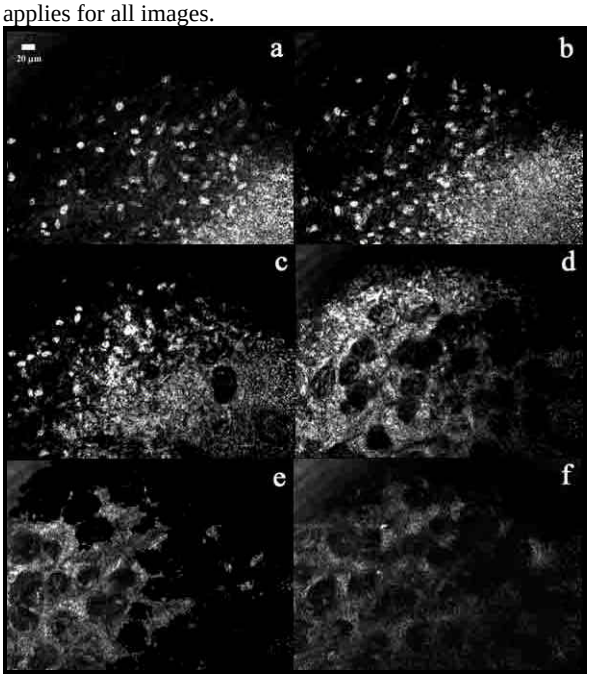

Figure 6. Images of a normal tissue area in a nude mouse, after the application of acetic acid. The brightness and contrast of each image has been increased by 50% and 30%, respectively. The field of view is 442 x 327 microns. Image (a) is 20 microns, (b) 40 microns, (c) 60 microns, (d) 80 microns, (e) 100 microns, and (f) 120 microns beneath the tissue surface. The scale bar in figure (a) applies for all images.

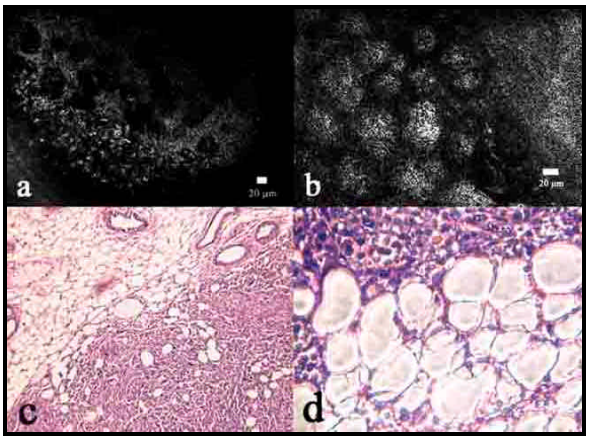

Figure 7. (a and b) Static images of adipocytes 100 microns below the imaging surface, after the application of acetic acid, from a nude and Balb/C mouse, respectively. The field of view for (a) is 676 x 502 microns and 380 x 262 microns for (b). (c and d) H&E stained sections of adipose tissue from the same Balb/C mouse, at 100x and 400x, respectively. The field of view is 898 x 704 microns for (c) and 225 x 176 microns for (d).

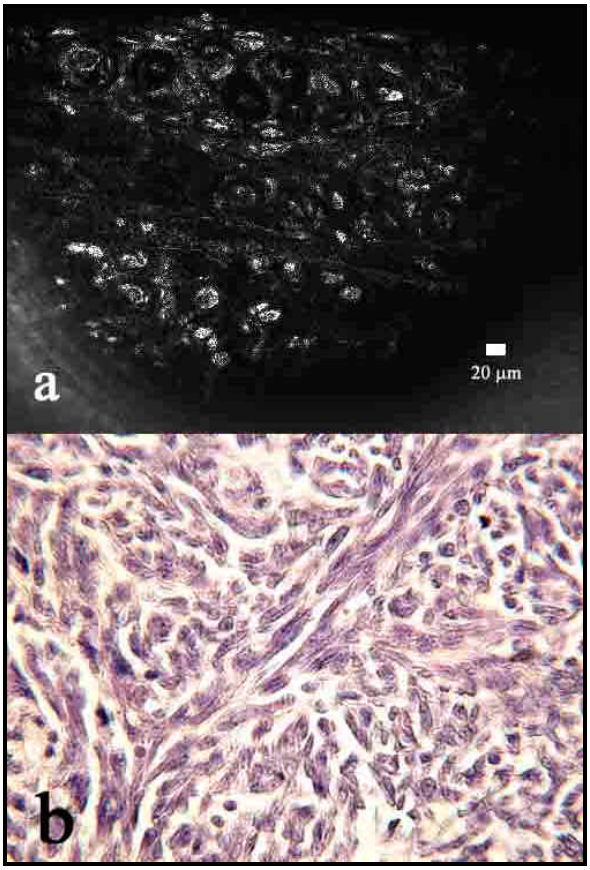

Figure 8. (a) Confocal image of tumor cells within a nude mouse 75 microns below the imaging surface, after the application of acetic acid. The field of view is 605 x 449 microns. (b) Image from H&E stained section of neoplastic tissue from the same nude mouse, at 400x. The field of view is 225 x 176 microns.

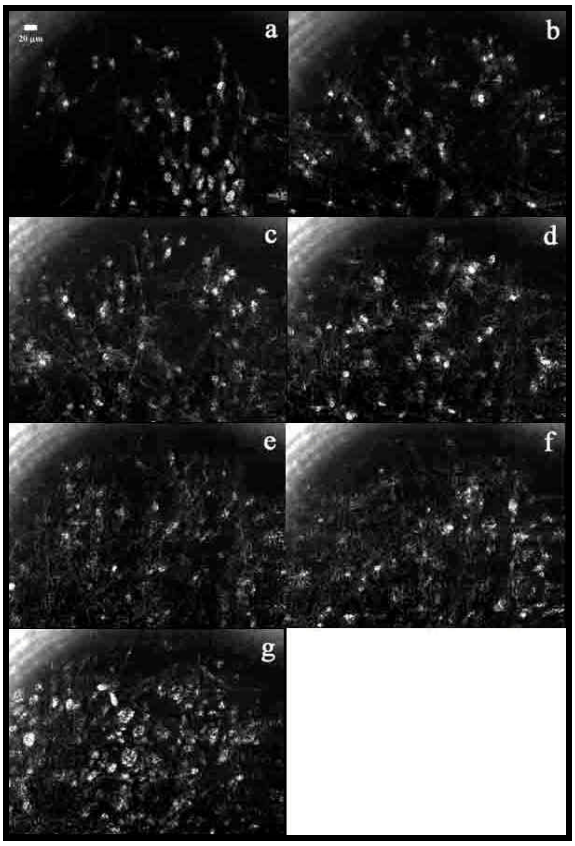

Figure 9. Images of a neoplastic tissue area in a nude mouse, after the application of acetic acid. The brightness of each image has been increased by 62% and contrast increased by 19%. The field of view is 442 x 327 microns. Image (a) is 200 microns, (b) 240 microns, (c) 260 microns, (d) 280 microns, (e) 300 microns, (f) 320 microns, and (g) 340 microns beneath the tumor surface. The scale bar in figure (a) applies for all images.

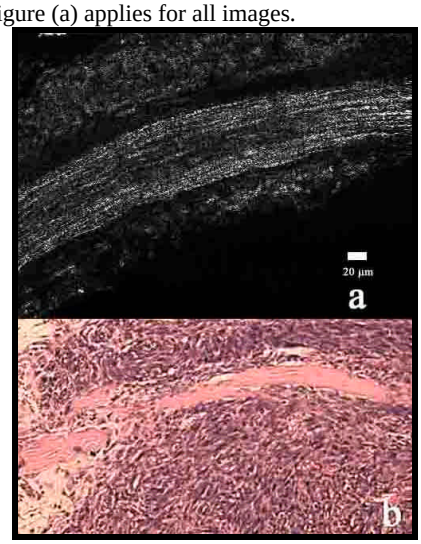

Figure 10. (a) Confocal image of striated muscle within the tumor of a Balb/C mouse, after adding acetic acid. Field of view is 426 x 315 microns. (b) Image from H&E stained section of neoplastic tissue from a nude mouse, at100x. The field of view is 268 x 147 microns.

reflectance-based confocal system we were able to obtain *in vivo* images and videos of the mouse mammary tumors with high lateral and axial resolutions. We were able to differentiate between normal and abnormal tissue areas within the mammary gland, including areas of adipose tissue, fibroblasts and connective tissue, neoplastic tissue, and blood flow within blood vessels. The confocal images of these tissues correspond well with H&E stained tissue slices from similar areas. The average depth of penetration ranged from 155 microns to greater than 300 microns, varying greatly with the size of the tumor and thickness of the encapsulating fibrous capsule.

Intravital imaging with reflectance confocal microscopy appears to be a useful tool for studying tumor cell behavior, which can be expanded to study tumor metastasis *in vivo*. Using reflectance, rather than fluorescence, we avoid the need to label the cancer cells with a fluorescent protein, looking instead at the natural backscattering from the cells. We hope to be able to utilize intravital imaging to specifically characterize breast cancer cell invasion during metastasis in future studies.

6. ACKNOWLEDGEMENTS

We would like to acknowledge the National Institutes of Health for their support of this research (Grant #1 RO1 CA 82880-01). We would also like to thank Galina Kiriakova for her assistance with the use and care of the mice.

7. REFERENCES

1. American Cancer Society. http://www.cancer.org.

2. Price, J. E.: Analyzing the metastatic phenotype. *J Cell Biochem* 56, 16-22 (1994)

3. Chambers, A. F.: The metastatic process: basic research and clinical implications. *Oncology Res* 11, 161-168 (1999)

4. Condeelis, J. S., J. Wyckoff, and J. E. Segall: Imaging of cancer invasion and metastasis using green fluorescent protein. *Eur J Cancer* 36, 1671-1680 (2000)

5. Moustafa, A. S., and G. L. Nicolson: Breast cancer metastasis associated genes: Prognostic significance and therapeutic implications. *Oncology Res* 9, 505-525 (1997)

6. Wyckoff, J. B., J. G. Jones, J. S. Condeelis, and J. E. Segall: A critical step in metastasis: *In vivo* analysis of intravasation at the primary tumor. *Cancer Res* 60, 2504-2511 (2000)

7. Mac Donald, I. C., E. E. Schmidt, V. L. Morris, A. C. Groom, and A. F. Chambers: *In vivo* videomicroscopy of experimental hematogenous metastasis: Cancer cell arrest, extravasation, and migration. In: *Motion Analysis of Living Cells.* Eds: Soll, D. and Wessels, D. John-Wiley & Sons, New York (1998)

8. Chambers, A. F., I. C. MacDonald, E. E. Schmidt, V. L. Morris, and A. C. Groom: Preclinical assessment of anti-cancer therapeutic strategies using *in vivo* videomicroscopy. *Cancer Met Rev* 17, 263-269 (1999)

9. Morris, V. L., I. C. MacDonald, S. Koop, E. E. Schmidt, A. F. Chambers, and A. C. Groom: Early interactions of cancer cells with the microvasculature in mouse liver and muscle during hematogenous metastasis: Videomicroscopic analysis. *Clin Exp Met* 11, 377-390 (1993)

10. Naumov, G. N., S. M. Wilson, I. C. MacDonald, E. E. Schmidt, V. L. Morris, A. C. Groom, R. M. Hoffman, and A. F. Chambers: Cellular expression of green fluorescent protein, coupled with high-resolution *in vivo* videomicroscopy, to monitor steps in tumor metastasis. *J Cell Sci* 112, 1835-1842 (1999)

11. MacDonald, I. C., E. E. Schmidt, V. L. Morris, A. F. Chambers, and A. C. Groom: Intravital videomicroscopy of the chorioallantoic microcirculation: A model system for studying metastasis. *Microvascular Res* 44, 185-199 (1992)

12. Farina, K. L., J. B. Wyckoff, J. Rivera, H. Le, J. E. Segall, J. S. Condeelis, and J. G. Jones: Cell motility of tumor cells visualized in living intact primary tumors using green fluorescent protein. *Cancer Res* 58, 2528-2532 (1998)

13. Wyckoff, J. B., J. E. Segall, and J. S. Condeelis: The collection of motile population of cells from a living tumor. *Cancer Res* 60, 5401-5404 (2000)

14. Jain, R. K.: Understanding barriers to drug delivery: High resolution *in vivo* imaging is key. *Clin Cancer Res* 5, 1605-1606 (1999)

15. Collier, T., P. Shen, B. de Pradier, K. Sung, and R. Richards-Kortum: Near real time confocal microscopy of amelanotic tissue: dynamics of aceto-whitening enable nuclear segmentation. *Opt Exp* 6, 40-48 (2000)

16. Miller, F. R., B. E. Miller, and G. H. Heppner: Characterization of metastatic heterogeneity among subpopulations of a single mouse mammary tumor: Heterogeneity in phenotypic stability. *Invasion Met* 3, 22-31 (1983)

17. Lachman, L. B., B. Ozpolat, X-M. Rao, G. Kiriakova, and J. E. Price: DNA vaccination against HER2/neu reduces breast cancer incidence and metastasis. *Cancer Gene Therapy* 8, 259-268 (2001)

18. Astoul, P., H. G. Colt, X. Wang, C. Boutin, and R. M. Hoffman: 'Patient-like' nude mouse metastatic model of advanced human pleural cancer. *J Cell Biochem* 56, 9-15 (1994)

19. Kubota, T.: Metastatic models of human cancer xenografted in the nude mouse: The importance of orthotopic transplantation. *J Cell Biochem* 56, 4-8 (1994)

Abbreviations: GFP: Green fluorescent protein; H&E: Hemotoxylin And Eosin

Key words: Biological imaging, Confocal microscopy, Medical imaging, Mouse model

Send correspondence to: Alicia Lacy, Department of Biomedical Engineering, ENS 610, The University of Texas at Austin, Austin, TX 78712, Tel: 512-471-3619, Fax: 512-475-8854 E-mail: a.lacy@mail.utexas.edu